DYNAMIC MAGNETIC RESONANCE ELASTOGRAPHY

Armando Manduca

Mayo Clinic College of Medicine

1. INTRODUCTION

There is strong precedent in clinical medicine for the concept that tissue viscoelastic properties, assessed by palpation, are markedly affected by a variety of disease processes. Student physicians learn that the presence of a hard mass in the thyroid, breast, or prostate is suspicious for malignancy. Indeed, many tumors of these structures are still first detected by touch. It is not uncommon for surgeons at the time of laparotomy to palpate tumors that were undetected in preoperative imaging by CT, MRI, or ultrasound. None of these modalities provide the information about the elastic properties of tissue elicited by palpation. The elastic moduli of various human soft tissues vary over a wide range (more than 4 orders of magnitude). In contrast, most of the physical properties depicted by conventional medical imaging modalities are distributed over a much smaller numerical range.
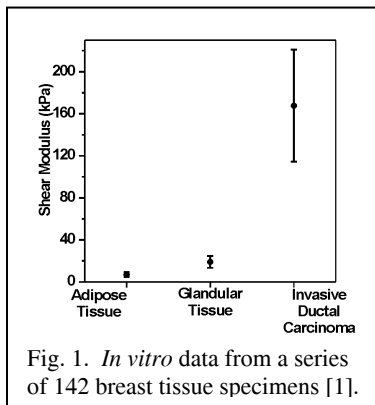

Fig. 1. *In vitro* data from a series of 142 breast tissue specimens [1].

The literature on the mechanical properties of abnormal tissues is limited. Nevertheless, data from breast tissue specimens have consistently shown that the measured shear moduli of various types of carcinomas are much higher than the shear moduli of normal adipose-glandular tissue (Fig. 1, [1-3]). Research has also suggested that pre-cancerous tissue changes are associated with alterations in mechanical properties [4,5]. It is also known that elastic moduli of many tissues can vary widely in response to changes in physiologic state [1,6]. For instance, the elasticity of muscle in the relaxed and contracted state can differ by more than 100-fold [6]. It is generally agreed that no other physical parameter of tissue is changed by pathological or physiological process to as great an extent as its elasticity.

These observations provide motivation for seeking a medical imaging technology that can depict the mechanical properties of tissues. Such a technology might: (1) provide a means to non-invasively "palpate" regions of the body that are beyond the reach of the physician's hand, (2) delineate tumors before they are large enough to detect by touch, (3) provide greater sensitivity for assessing changes in tissue elasticity, and (4) provide a useful new quantitative tool for characterizing tissue. Magnetic resonance elastography (MRE) is a phase contrast based MRI imaging technique that can directly visualize and quantitatively measure propagating acoustic strain waves in tissue-like materials subjected to harmonic mechanical excitation. The data acquired allows the calculation of local quantitative values of shear modulus and the generation of images that depict tissue elasticity or stiffness. MRE thus shows promise as a potential technique for "palpation by imaging", with possible applications in tumor detection, disease characterization and assessment of rehabilitation (particularly in muscle).

2. ELASTIC PROPERTIES OF SOFT TISSUE

In isotropic materials, the proportionality constant that describes the amount of longitudinal deformation (expressed in terms of strain) that occurs in a given material in response to an applied longitudinal force (expressed in terms of stress) is known as *Young's modulus (E)* of elasticity. The *first Lame constant* (λ) relates transverse strain to longitudinal stress, and the *second Lame constant* or *shear modulus* (μ) relates shear strain to shear stress. The *bulk modulus (K)* of elasticity describes the change in volume of a material to external stress. Finally, *Poisson's ratio (v)* is the ratio of transverse contraction per unit breadth divided by longitudinal extension per unit length. These parameters are interrelated, so that knowledge of any two allows calculation of the other three.

Most soft tissues have mechanical properties that are intermediate between those of fluids and solids. The value of Poisson's ratio for soft tissues, which can be directly calculated from the ratio of longitudinal and shear wave speeds, is on the order of $v = 0.499999$, very close to the value for liquids ($v = 0.5$). This implies that soft tissues are very nearly incompressible, and that Young's modulus and shear modulus differ only by a scaling factor ($E = 3\mu$). In contrast to the many orders of magnitude over which the Young's and shear moduli are distributed, the bulk moduli of most soft tissues differ by less than 15% from that of water [7]. The density of soft tissue also differs little from that of water [8].

These concepts represent a simplification of the mechanical behavior of soft tissues, which in general can be anisotropic, non-Hookean, and viscoelastic.

3. ELASTICITY IMAGING TECHNIQUES

Much of the pioneering work in elasticity imaging has been accomplished using ultrasound and either a quasi-static stress model [9-13] or a dynamic stress model [14-19]. The quasi-static stress method employs an ultrasound transducer to apply a small axial compression to tissue. Sonograms obtained without and with compression are correlated to determine the displacement at each location, thereby revealing the longitudinal strain distribution. Images depicting this local strain estimate have been shown to provide an informative qualitative depiction of the elasticity of materials in tissue-simulating phantoms and surgical tissue specimens [20]. *In vivo* studies of the method have demonstrated the feasibility of delineating breast cancer [9,21] by elastography. Such images can also be processed to compute a quantitative map of regional elastic modulus (*E*), but this calculation requires an estimate of local stress distribution, which in turn depends on the spatial composition of the object and knowledge of the applied stress distribution [11-13].

The sonoelasticity method developed by Parker *et al.* employs a vibrational mechanical stress, typically in the range of 20-400 Hz [14-19]. Tissue is imaged with Doppler ultrasonography to observe the regional amplitude of the resulting standing wave pattern. Structures with high elastic moduli tend to have lower vibrational amplitudes than surrounding softer tissues. An *in vitro* study of excised prostates has demonstrated that this qualitative technique delineates adenocarcinoma with higher sensitivity than conventional sonographic imaging [19]. A related method has employed Doppler ultrasound in an attempt to map the pattern of propagating mechanical waves in phantoms, animal tissue, and in the human liver [22,23]. Other approaches for elasticity imaging employ ultrasound radiation force as a source of quasistatic stress [24,25], or perform transient imaging of shear waves with an ultra-fast scanner [26,27].

In MRI, saturation tagging methods have been employed in applications as diverse as evaluating the local motion of cardiac muscle [28,29] and observing connective motion in vibrated granular material [30]. A grid of saturation tags can be applied to tissue before it is deformed by an applied static stress [31]. The pattern of deformation of the grid of saturation tags can then be analyzed to provide a map of local strain. Local motion can also be measured with motion-encoded phase contrast imaging. This has been used clinically in applications such as assessing regional myocardial motion, CSF pulsation, and intravascular blood flow [32-34]. Plewes *et al.* proposed a method for elastography involving use of a phase contrast imaging sequence to estimate the spatial strain distribution resulting from a small quasi-static longitudinal stress, applied once each time the pulse sequence is repeated [35-37]. Phantom studies showed that the strain maps allow distinction of an object with high stiffness from surrounding softer material. A quantitative determination of regional elastic modulus can be calculated given an estimation of the regional distribution of stress.

Dynamic MR elastography (MRE) uses harmonic mechanical excitation rather than static stress as a probe [38,39]. Shear waves at frequencies in the 50-1000 Hz range are suitable as a probe because they are much less attenuated than at higher frequencies, their wavelength in tissue-like materials is in the useful range of millimeters to tens of millimeters, and because shear modulus varies widely in bodily tissues. High frequency longitudinal waves (ultrasound) are not directly suitable for use as a probe, because their propagation is governed by the bulk modulus, which varies little in soft tissue. Longitudinal acoustic waves at lower frequencies are also not suitable because of their long wavelength (on the order of meters below 1 kHz [7]).
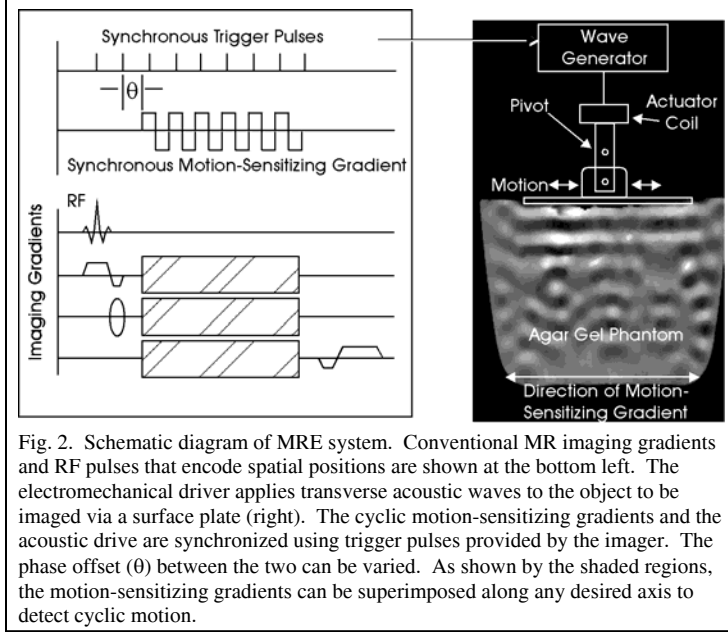
4. MAGNETIC RESONANCE ELASTOGRAPHY (MRE)

In dynamic MRE, a phase-contrast MRI technique is used to spatially map and measure displacement patterns corresponding to harmonic shear waves with amplitudes of microns or less. A conventional MRI system is used with an additional motion-sensitizing gradient imposed along a specific direction, switched in polarity at some adjustable frequency [40,41]. Trigger pulses synchronize an oscillator/amplifier unit that drives an electromechanical actuator coupled to the surface of the object to be imaged, inducing shear waves in the object at the same frequency as the motion-sensitizing gradient (Fig. 2, [R39]). Any cyclic motion of the spins in the presence of these motion-sensitizing gradients causes a measurable phase shift in the received MR signal. From the measured phase shift, it is possible to calculate the displacement at each voxel, and directly image the acoustic waves within the object. Extreme sensitivity to small amplitude synchronous motion can be achieved by accumulating phase shifts over multiple cycles of mechanical excitation and the motion-sensitizing gradient waveform.

The phase shift caused by a propagating mechanical wave with a wave vector k within a medium at a given frequency (1/T) in the presence of a cyclic motion-encoding gradient is given by [38,39]:

$$\phi(\vec{r}, \theta) = \frac{\gamma NT(\vec{G}_o \bullet \vec{\xi}_0)}{2} \cos(\vec{k} \bullet \vec{r} + \theta) \qquad (1)$$

This accumulated phase shift is proportional to the dot product of the displacement amplitude vector $\vec{\xi}_0$ and the motion-sensitizing magnetic gradient vector $\vec{G}$, and the relative phase θ of the mechanical and magnetic oscillations. Particles whose component of motion along the gradient vector are exactly in phase or out of phase with the magnetic oscillation have maximum phase shifts of opposing polarities. Particles whose component of motion along the gradient vector is 90 degrees out of phase with it have no net phase shift. The response is also proportional to the number of gradient cycles (N) and the period of the gradient waveform (T). The quantity γ is the gyromagnetic ratio and $\vec{r}$ is the spin position vector.

Fig. 2. Schematic diagram of MRE system. Conventional MR imaging gradients and RF pulses that encode spatial positions are shown at the bottom left. The electromechanical driver applies transverse acoustic waves to the object to be imaged via a surface plate (right). The cyclic motion-sensitizing gradients and the acoustic drive are synchronized using trigger pulses provided by the imager. The phase offset (θ) between the two can be varied. As shown by the shaded regions, the motion-sensitizing gradients can be superimposed along any desired axis to detect cyclic motion.

Generally, two acquisitions are made for each repetition, reversing the polarity of the motion sensitizing gradients. This reduces systematic phase errors and doubles the sensitivity to small displacements. The number of gradient pulses (N) typically varies from 2-30 cycles and the frequency of mechanical excitation ranges from 50-1000 Hz. Acquiring and processing 2D slices captures only two of the three components of the wave propagation vector, and may yield misleading results unless the shear wave is propagating in plane, but time considerations or other factors may mandate their use. 3D MRE pulse sequences have also been developed [42-44] but require acquisition times of tens of minutes.

The resulting phase difference images reflect the displacement of spins due to acoustic strain wave propagation in the medium and are termed "wave images". Such an image of propagating acoustic waves in a tissue-simulating agarose gel phantom is shown in Figure 3. The wave propagation depends on the elasticity of the material at each location in the object, allowing the construction of elastograms as shown. Experiments to assess the sensitivity of the shear wave imaging method at low amplitudes of mechanical excitation demonstrated that displacements of less than 100 nanometers can be readily observed [38].
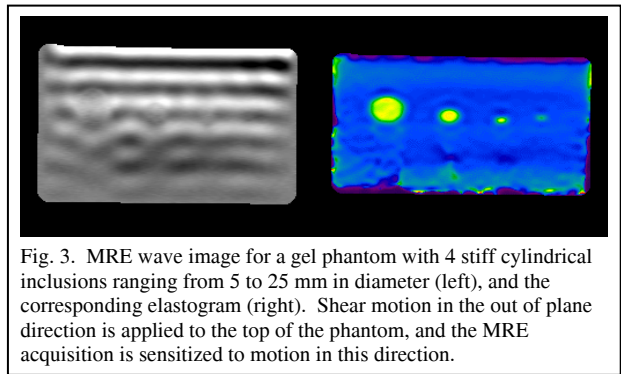
A moving-coil driver is commonly used for mechanical excitation, with the imager providing the static magnetic field. Piezoelectric drivers can also be used for generating shear waves, and the mechanical excitation can also be applied longitudinally, with mode conversion leading to shear waves being generated inside the object [43,44]. Modulated focused ultrasound can also generate shear waves that can be imaged with MRE [45].

Fig. 3. MRE wave image for a gel phantom with 4 stiff cylindrical inclusions ranging from 5 to 25 mm in diameter (left), and the corresponding elastogram (right). Shear motion in the out of plane direction is applied to the top of the phantom, and the MRE acquisition is sensitized to motion in this direction.

By adjusting the phase offset between the mechanical excitation and the oscillating magnetic gradient (θ in Fig. 2), acoustic wave images can be obtained at various phase offsets (typically 4 to 8) regularly spaced around a cycle. This allows extraction of the harmonic component at the frequency of interest, giving the amplitude and the phase (relative to an arbitrary zero point) of the harmonic displacement at each point in space [46]. This extraction also provides some degree of noise reduction and allows visualization of wave propagation as a cine loop.

A single MRE acquisition is sensitized to motion in a single direction. However, the experiment can be repeated and the sensitization direction varied to capture all three orthogonal components of displacement. Thus, MRE can acquire full 3D cyclic displacement information at MR pixel resolution throughout a 3D volume. In principle, this

makes it feasible to estimate all components of the strain tensor, thereby making it possible to probe the anisotropic mechanical properties of tissues [38,39,43,47].

MRE is highly sensitive only to motion that is precisely synchronized with the sensitization gradients, and is no more sensitive to physiologic motion than a conventional gradient echo sequence [48]. Sensitivity to non-synchronous motion can be further reduced by explicitly nulling the individual moments of the gradient waveform. It is also possible to modulate the envelope of the motion encoding waveform to further increase its spectral selectivity [49].

In summary, MRE offers: direct visualization and quantitative measurement of tissue displacements, high sensitivity to very small motions, a field of view unencumbered by acoustic window requirements, and the ability to obtain full 3D displacement data throughout a 3D volume. With some assumptions (below), this allows direct local inversion of the data to recover elasticity, with no need for boundary conditions or the estimation of a stress field.

5. DATA PROCESSING

A linear relationship between stress and strain can generally be assumed in MRE since the displacements are very small (typically 1-50 microns). In the general case, stress and strain are related by a rank 4 tensor with up to 21 independent quantities [50]. If the material is assumed to be isotropic, this reduces to two independent quantities (the Lame constants λ and μ in our formulation). If one also assumes local homogeneity, λ and μ become single unknowns within small local regions, and the general equation for harmonic motion becomes an algebraic matrix equation that can be solved locally by matrix inversion [51,52]:

$$\mu\nabla^2\mathbf{u} + (\lambda + \mu)\nabla(\nabla\cdot\mathbf{u}) = -\rho\omega^2\mathbf{u} \qquad (2)$$

with ρ the density of the material, ω the angular frequency of the mechanical oscillation, and $\mathbf{u}$ the displacement vector. Solving this equation requires knowledge of the full 3D displacement, since the equations for the individual components are coupled. In soft tissues, $\lambda \gg \mu$ (typically 10^4 or more), and the longitudonal wavelength is so long (tens of meters) that accurate estimation of λ is very challenging. However, it is possible to filter out the longitudonal wave field by suppressing very low spatial frequencies, performing a Helmholtz decomposition of the vector field [53], or taking the curl of the displacement [51,54]. If one assumes incompressibility (a very good assumption for soft tissue) and performs such filtering the equation then simplifies to the Helmholtz equation:

$$\mu\nabla^2\mathbf{u} = -\rho\omega^2\mathbf{u} \qquad (3)$$

The components in the different orthogonal directions are now decoupled, and each component satisfies the equation separately. Thus, measurements in only one sensitization direction suffice to determine μ.

The Lame constants can be considered to be complex quantities, with the imaginary parts of the constants representing attenuation for a viscoelastic medium. The true "shear modulus" is the real part μ_r, which describes the behavior of a static object in equilibrium. When μ_i is non-zero, the wave speed is a function of frequency (dispersion). In practice, it is difficult to estimate μ_i since it is more sensitive to noise, but estimates of the wave speed are more robust. Quantities reported below are typically an "effective" shear modulus or *shear stiffness* at the frequency ω (if $\rho = 1.0$, this is simply the wave speed squared). The spatial wavelength decreases and attenuation increases as the mechanical frequency increases. This yields higher resolution, since the wavelength is smaller, but lower SNR due to higher attenuation. The best frequency for a particular application depends on this tradeoff.

A variety of inversion techniques have been proposed for Helmholtz inversion [52]. *Direct inversion* uses filtered estimates of displacement and its Laplacian in a local neighborhood to solve for μ at each point in the image or volume [51,52,55,56]. *Local frequency estimation* combines local estimates of instantaneous frequency over several scales [57,58] and is effectively solving the Helmholtz equation under the assumption of no attenuation [59]. These techniques depend simply on the presence of sufficient motion within the local region, and in principle correctly handle complex interference patterns from reflection, refraction, etc. However, difficulties can arise in areas of low displacement amplitude and hence low SNR caused by these situations. A simpler, unrelated inversion technique, *phase gradient*, assumes propagation of a single shear wave, and simply calculates the gradient of its phase [46,52]. This technique breaks down with wave superposition (reflection, interference, etc.), and its use to date is limited to specialized situations. A spatio-temporal directional filter can be applied as a pre-processing step to separate complex wave fields into components propagating in different directions, each of which can be analyzed separately [60], resulting in improved inversions with all of the above techniques.

The resolution of MRE inversion is limited by the accuracy of the spatial derivative estimation, and thus ultimately by the SNR (noisy data requires estimation over larger spatial windows). Stiffer objects are more difficult to estimate accurately since their spatial derivatives of displacement are smaller. Higher SNR is obtained by (1) larger underlying MR magnitude signal, and (2) larger displacement amplitude. Since shear waves attenuate quickly in certain tissues, large amplitudes of motion near the surface may be required to achieve sufficient amplitude in a deep region of interest. Too much amplitude can cause phase wrap; however, standard phase unwrapping algorithms [61] can be applied to MRE data with good success. Quantitative measurements of shear modulus with MRE have shown high correlation with measurements using biomechanical testing devices [38,62,63].

Van Houten *et al.* [44,64,65] have described a finite element based technique for inverting MRE data. A solution is iteratively refined on small overlapping subzones of the overall domain, by updating the solution based on differences between forward calculations of displacement from the current solution and measured values. Local homogeneity is not assumed. This approach is computationally very intensive. Sinkus *et al*. [43,66] have proposed techniques that attempt to solve, in a limited way, for anisotropic characteristics of tissue. These techniques use full 3D sensitization and volume acquisitions, and apply longitudinal driving to *in vivo* breast tissue [43,44,66].

Tissue in general shows non-linear behavior, and the stress-strain curve for large displacements deviates considerably from a straight line. MRE displacements are usually small enough that behavior is linear, and the stiffness represents the slope of the stress-strain curve at the experimental conditions. However, the amount of compression applied to the tissue (by the mechanical driver, or by other aspects of the experiment) can determine where the stress-strain curve is being probed, and different experiments on the same tissue can report different stiffness values. Samani *et al.* [67] model this behavior with hyperelastic parameters, and have proposed an inversion scheme that attempts to recover these and use the entire stress-strain curve for material characterization.

6. APPLICATIONS

Ex vivo animal tissues

MRE can quantitatively assess the viscoelastic properties of real tissues and detect changes in stiffness with frequency and temperature [47]. For example, the calculated shear stiffness of porcine liver tissue at different mechanical frequencies are well fit by a viscoelastic model, and bovine skeletal muscle became softer with increasing temperature in the range of 20-45°C [47]. Due to the lack of metabolic activity, homeostatis, and *in situ* preloading in specimens, the observed mechanical properties are likely to be different than those that would be measured *in vivo*.

Breast

Various groups have reported MRE results on *in vivo* human breast [37,43,44,53,66,68,69]. Clear distinction has been found between fat and glandular tissues [44,69], in rough agreement with earlier results on excised tissue, and between normal breast tissue and carcinoma [53,66,68,69]. Fig. 4 illustrates differentiation between adipose and glandular tissue in the elastogram of a normal volunteer. Fig. 5 shows an area of high stiffness in the elastogram of a patient with biopsy-proven breast cancer corresponding to the location of the tumor.
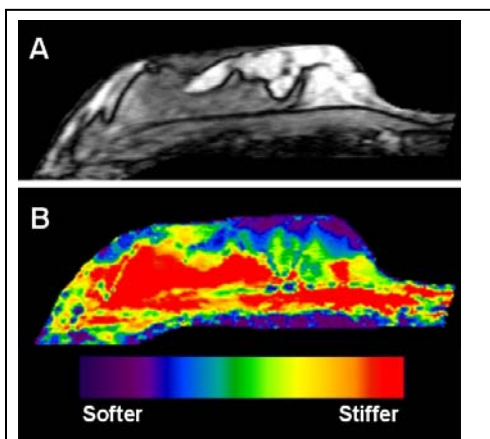

Fig. 4. (a) Axial T1 weighted spin-echo image of the breast of a normal volunteer. (b) MR elastogram obtained with shear waves at 100 Hz applied to the anterior of the breast, showing differentiation between soft adipose tissue and stiffer fibroglandular tissue.
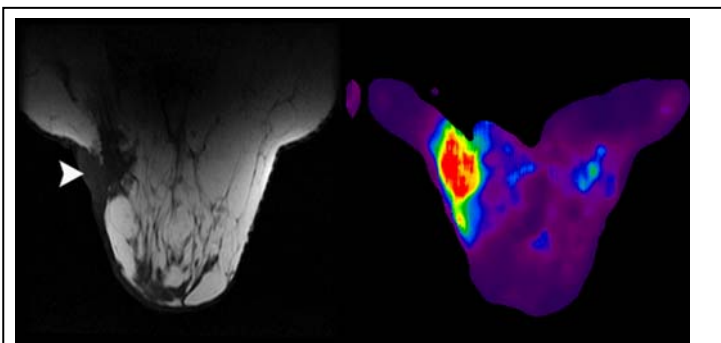

Fig. 5. MR elastogram of the breast of a patient with a 4 cm diameter, biopsy-proven breast cancer. The image was obtained with shear waves at 100 Hz, applied to the skin of the medial and lateral aspects of the breast. The field of view is 16 cm and the thickness is 5 mm. The shear stiffness of the tumor (arrowhead) is substantially higher than that of normal fibroglandular and adipose tissues in the breast.

Brain

While there is no clinical precedent for "brain palpation", it is possible that measurements of elastic properties might be useful for characterizing brain disease, as well as being necessary prerequisites for finite element studies of brain trauma and surgical simulation. MRE studies indicate that the *in vivo* shear stiffness of white matter (average 14.2 kPa) is higher than that of gray matter (average 5.3 kPa) [70]. Fig. 6 shows results for a normal volunteer, illustrating some correspondence with anatomy along the outer gray/white tissue boundary. The "hot spots" in the interior are artifacts due to high attenuation giving very low displacement amplitudes.
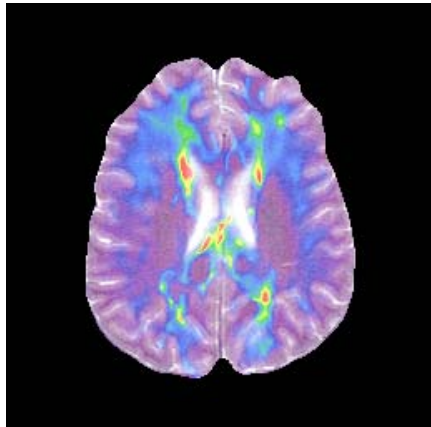

Fig. 6. An elastogram of the brain of a normal volunteer overlaid on the MR magnitude image.
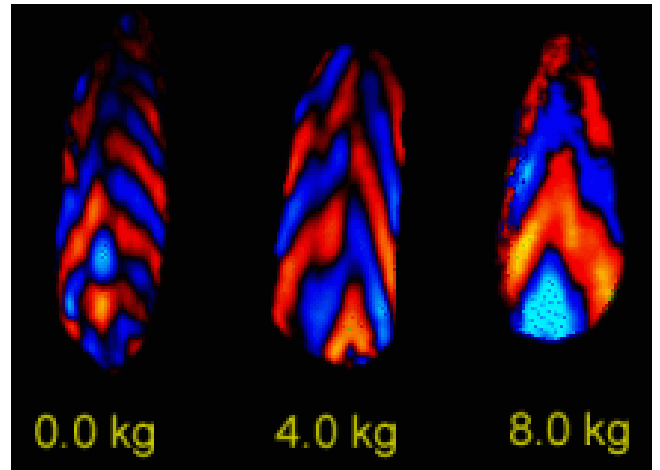

Fig. 7. Wave images obtained in a coronal plane through the biceps of a volunteer under the loading conditions indicated. Shear waves at 150 Hz were generated by a driver over the distal biceps tendon (bottom). The wave image, sensitized for out of plane motion, demonstrates propagating waves and a shear wavelength that increases with load.

Muscle

MRE has been applied to skeletal muscle to quantify the change in stiffness with muscle loading [71]. The wavelength of the shear wave increases with load (Fig. 7), and the shear stiffness of the muscle rises approximately linearly with force. Methods to determine anisotropic elastic constants for muscle [72] and for analyzing guided wave propagation along muscle fibers [53] have been proposed.

Liver

MRE is being studied as a non-invasive technique for the assessment of liver fibrosis. Recent studies have demonstrated that shear stiffness, as determined by MRE, increases with increasing stage of fibrosis, with one study yielding mean values ranging from 2.0 kPa for normal volunteers to 6.58 kPa for patients with biopsy-proven fibrosis [73], and another yielding mean values of 2.2 kPa for patients without substantial fibrosis (stages F0-F1) and 4.68 kPa for patients with cirrhosis (stage F4) [74].

Ultrasound Wave Field Visualization

Walker et al. have used specially constructed apparatus to image ultrasound wave fields with MRE. Nanometer motions at ultrasonic frequencies were clearly detected, and direct measurements of absolute pressure, intensity, and speed of sound were obtained [75]. Although the magnetic field gradients required are an order of magnitude greater than the recommended limits for human imaging, this technique allows the detailed study of ultrasound propagation and scattering in heterogeneous ex vivo tissue samples.

Characterization of Thermally Ablated Tissue

Studies have demonstrated that MRE delineates thermally coagulated tissues as areas of increased shear stiffness [45,76]. MRE performed at multiple times during heating and cooling of bovine tissue has revealed a characteristic irreversible change in tissue shear stiffness that appears to correspond to tissue coagulation.

9. CONCLUSION

MRE is capable of non-invasive *in vivo* determination of mechanical properties in a variety of tissues. The detection of propagating acoustic waves has been demonstrated *ex vivo* and *in vivo* in numerous animal and human tissues. Reconstruction algorithms have been validated and yield quantitative measures of elasticity that clearly demarcate differences between tissue types and identify tumors as areas of higher stiffness. Challenges remain in pulse sequence design, mechanical driver design, and improving processing algorithms to generate more accurate, higher

resolution elasticity and viscosity maps. MRE may prove to be useful in tumor detection, tissue and disease characterization, and the evaluation of rehabilitation.

REFERENCES

1.   Sarvazyan A, et al. (1994). Elasticity Imaging as a new modality of medical imaging for cancer detection, Proc. Intl. Workshop on Interaction of Ultrasound with Biological Media Valenciennes, France. p. 69-81.
2.   Burke, TM, Blankenberg, TA, Sui, AKQ, Blankenberg, FG and Jensen, HM (1990). Preliminary results for shear wave speed of sound and attenuation coefficients from excised specimens of human breast tissue. Ultrason Img 12:99-118.
3.   Krouskop, TA, Wheeler, TM, Kallel, F et al. (1998). Elastic moduli of breast and prostate tissues under compression. Ultrasn Img 20:260-74.
4.   Sarvazyan A (1993). Shear acoustic properties of soft biological tissues in medical diagnostics. 125th Mtg, Acoust Soc America, p. 2329.
5.   Burke TM, Blankenberg TA, Sui AKQ, Blankenberg FG, Jensen HM (1990). Preliminary results for shear wave speed of sound and attenuation coefficients from excised specimens of human breast tissue. Ultrason Img 12:99-118.
6.   Duck FA (1990). Physical Properties of Tissues – A Comprehensive Reference Book. 6th ed. Academic Press.
7.   Goss SA, Johnston RL, Dunn F (1978). Comprehensive compilation of empirical ultrasonic properties of mammalian tissues. J Acoust Soc America 64:423-57.
8.   Burlew, MM, Madsen, EL, Zagzebski, JA et al. (1980). A new ultrasound tissue-equivalent material. Radiology 134(2):517-520.
9.   Ophir J, Cespedes I, Ponnekanti H, Yazdi Y, Li X (1991). Elastography: a quantitative method for imaging the elasticity of biological tissues. Ultrason Img 13(2):111-134.
10. Cespedes I, Ophir J, Ponnekanti H, Maklad N (1993). Elastography: elasticity imaging using ultrasound with application to muscle and breast in vivo. Ultrason Img 15:73-88.
11. Ponnekanti H, Ophir J, Cespedes I (1992). Axial stress distributions between coaxial compressors in elastography: an analytical model. Ultrasound Med Bio 18:667-73.
12. Ponnekanti H, Ophir J, Cespedes I (1994). Ultrasonic-Imaging of the stress-distribution in elastic media due to an external compressor. Ultrasound Med Bio 20:27-33.
13. Ponnekanti H, Ophir J, Huang Y, Cespedes I (1995). Fundamental mechanical limitations on the visualization of elasticity contrast in elastography. Ultrasound Med Bio 21:533-543.
14. Gao L, Parker KJ, Alam SK, Lerner RM (1995). Sonoelasticity imaging - theory and experimental-verification. J Acoust Soc America 97: 3875-3886.
15. Lee F, Jr., Bronson JP, Lerner RM et al. (1991). Sonoelasticity imaging: results in in vitro tissue specimens. Radiology 181:237-239.
16. Lerner RM, Huang SR, Parker KJ (1990). Sonoelasticity images derived from ultrasound signals in mechanically vibrated tissues. Ultrasound in Medicine and Biology 16:231-239.
17. Parker KJ, Huang SR, Musulin RA, Lerner RM (1990). Tissue Response to mechanical vibrations for 'sonoelasticity imaging'. Ultrasound in Medicine and Biology 16:241-246.
18. Parker KJ, Lerner RM (1992). Sonoelasticity of organs: shear waves ring a bell. J Ultrasound Med 11:387-392.
19. Rubens DJ, Hadley MA, Alam SK et al. (1995). Sonoelasticity imaging of prostate-cancer -in-vitro results. Radiology 195: 379-383.
20. Krouskop TA, Wheeler TM, Kallel F, Garra BS, Hall T (1998). Elastic moduli of breast and prostate tissues under compression. Ultrason Img 20: 260-274.
21. Garra BS, Cespedes EI, Ophir J et al. (1997). Elastography of breast lesions: Initial clinical results. Radiology 202:79-86.
22. Yamakoshi Y, Sato J, Sato I (1990). Ultrasound imaging of internal vibration of soft tissue under forced vibration. IEEE Trans Ultra Ferr Freq Ctl 37:45-53.
23. Krouskop TA, Dougherty DR, Vinson FS (1987). A pulsed Doppler ultrasonic system for making noninvasive measurements of the mechanical properties of soft tissue. J Rehabilitation Research Development 24: 1-8.
24. Nightingale KR, Palmeri ML, Nightingale RW, Trahey GE (2001). On the feasibility of remote palpation using acoustic radiation force. J Acoust Soc America 110:625-634.
25. Nightingale KR, Soo MS, Nightingale R, Trahey G (2002). Acoustic radiation force impulse imaging: in vivo demonstration of clinical feasibility. Ultrasound Med Bio 28::227-235.
26. Sandrin L, Tanter M, Catheline S, Fink M (2002). Shear modulus imaging with 2-D transient elastography. IEEE Trans. Ultra. Ferr. Freq. Cntrl. 49:426-435.
27. Gennisson JL, Catheline S, Chaffai S, Fink M (2003). Transient elastography in anisotropic medium: application to the measurement of slow and fast shear wave speeds in muscles. J. Acoust. Soc. Am. 114:536-541.
28. Axel L and Dougherty L (1989). MR imaging of motion with spatial modulation of magnetization. Radiology 171:841-845.
29. Zerhouni EA, Parish DM, Rogers WJ, Yang A, Shapiro EP (1988). Human heart: tagging with MR imaging-a method for noninvasive assessment of myocardial motion. Radiology 169:59-63.
30. Ehrichs EE, Jaeger HM, Karczmar GS et al. (1995). Granular convection observed by magnetic resonance imaging. Science 267:1632-1634.
31. Fowlkes JB, Emelianov SY, Pipe JG, Skovoroda AR, Carson PL, Adler RS, Sarvazyan AP (1995). Magnetic resonance imaging techniques for detection of elasticity variation. Med Phys 22: 1771-1778.
32. O'Donnell M (1985). NMR blood flow imaging using mutiecho, phase contrast sequences. Med Phys 12: 59-64.
33. Bernstein MA, Ikezaki Y (1991). Comparison of phase-difference and complex-difference processing in phase-contrast MR angiography. JMRI 1:725-729.
34. Pelc NJ, Shimakawa A, Glover GH (1989). Phase contrast cine MRI. Proc Soc MRM, p.101.
35. Plewes DB, Betty I, Urchuk SN, Soutar I (1994). Visualizing tissue compliance with MR. Proc Soc MRM, p.410.
36. Plewes DB, Betty I, Urchuk SN, Soutar I (1995). Visualizing tissue compliance with MR imaging. JMRI 5:733-738.
37. Plewes DB, Bishop J, Samani A, Sciarretta J (2000). Visualization and quantification of breast cancer biomechanical properties with magnetic resonance elastography. Phys Med Bio 45:1591-1610.
38. Muthupillai R, Lomas DJ, Rossman PJ, Greenleaf JF, Manduca A, Ehman RL (1995). Magnetic resonance elastography by direct visualization of propagating acoustic strain waves. Science 269:1854-1857.
39. Muthupillai R, Rossman PJ, Greenleaf JF, Riederer SJ, Ehman RL (1996). Magnetic resonance imaging of transverse acoustic strain waves. MRM 36: 266-274.
40. Callaghan PT, Stepisnik J. Frequency-domain analysis of spin motion using modulated-gradient NMR (1995). J Mag Res A 117:118-122.

41. Denk W, Keolian RM, Ogawa S, Jelinski LW (1993). Oscillatory flow in the cochlea visualized by a magnetic resonance imaging technique. Proc Natl Acad Sci 90:1595-1598.

42. Muthupillai R, Dutt V, Rossman PJ, Hulshizer TC, Manduca A and Ehman RL (1997). Three dimensional magnetic resonance elastography with multi-axis motion encoding. Proc ISMRM 5:460.

43. Sinkus R, Lorenzen J, Schrader D *et al*. (2000). High-resolution tensor MRE for breast tumor detection. Phys Med & Bio 45:1649-1664.

44. Van Houten EEW, Doyley MM, Kennedy FE, Weaver JB, Paulsen KD (2003). Initial in-vivo experience with steady-state subzone-based MR elastography of the human breast. JMRI 17:72-85.

45. Wu T, Felmlee JP, Greenleaf JF *et al*. (2000). MR imaging of shear waves generated by focused ultrasound. MRM 43:111-115.

46. Manduca A, Smith JA, Muthupillai R, Rossman PJ, Greenleaf JF and Ehman RL (1997). Image analysis techniques for magnetic resonance elastography. Proc ISMRM 5:1905.

47. Kruse SA, Smith JA, Lawrence AJ, Dresner MA, Manduca A, Greenleaf JF and Ehman RL (2000). Tissue characterization using magnetic resonance elastography: Preliminary results. Phys Med & Bio 45:1579-1590.

48. Muthupillai R, Rossman PJ, Greenleaf JF, Riederer SJ, Ehman RL (1996). MRI visualization of acoustic strain waves: Effect of linear motion. Proc ISMRM 4:1515.

49. Muthupillai R, Ehman RL (1997). Amplitude modulated cyclic gradient waveforms: applications in MRE. Proc ISMRM 6:1904.

50. Auld BA (1990). Acoustic Fields and Waves in Solids, Krieger Publishing Company, Malabar, Florida.

51. Oliphant TE, Manduca A, Ehman RL, Greenleaf JF (2001). Complex-valued stiffness reconstruction for magnetic resonance elastography by algebraic inversion of the differential equation. MRM 45:299-310.

52. Manduca A, Oliphant TE, Dresner MA, Mahowald JL, Kruse SA, Amromin E, Greenleaf JF, Ehman RL (2001). Magnetic resonance elastography: in vivo non-invasive mapping of tissue elasticity. Medical Image Analysis 5:237-254.

53. Romano AJ, Abraham PB, Rossman PJ, Bucaro JA, Ehman RL (2005). Determination and analysis of guided wave propagation using magnetic resonance elastography. MRM 54:893-900.

54. Sinkus R, Tanter M, Xydeas T, Catheline S, Bercoff J, Fink M (2005). Viscoelastic shear properties of in vivo breast lesions measured by MR elastography. Magn Reson Imaging. 23:159-65.

55. Romano AJ, Shirron JJ, Bucaro JA (1998). On the noninvasive determination of material parameters from a knowledge of elastic displacements: theory and numerical simulation. IEEE Trans Ultra Ferr Freq Ctl 45:751-759.

56. Romano AJ, Bucaro JA, Ehman RL, Shirron JJ (2000). Evaluation of a material parameter extraction algorithm using MRI- based displacement measurements. IEEE Trans Ultra Ferr Freq Ctl 47:1575-1581.

57. Knutsson H, Westin C-F and Granlund G (1994). Local multiscale frequency and bandwidth estimation. Proc IEEE Conf Img Proc 1:36-40.

58. Manduca A, Muthupillai R, Rossman PJ *et al*. (1996). Image processing for magnetic resonance elastography. SPIE Med Img 2710:616-623.

59. Oliphant TE (2001). Direct methods for dynamic elastography reconstructions: Optimal inversion of the interior Helmholtz problem. Ph.D. thesis, Mayo Graduate School.

60. Manduca A., Lake DS, Kruse, SA, Ehman, RL (2003). Spatio-temporal directional filtering for improved inversion of MR elastography images. Medical Image Analysis 7:465-473.

61. Ghiglia DC and Pritt MD (1998). Two-Dimensional Phase Unwrapping: Theory, Algorithms and Software, John Wiley & Sons, NY, USA

62. Hamhaber U, Grieshaber FA, Nagel JH, Klose U (2003). Comparison of quantitative shear-wave MR-elastography with mechanical compression tests. MRM 49:71-77.

63. Ringleb SI, Chen Q, Lake DS, Manduca A, Ehman RL, An K-N (2005). Quantitative Shear Wave Magnetic Resonance Elastography: Comparison to a Dynamic Shear Material Test. MRM 53:1197-1201.

64. Van Houten EEW, Paulsen KD, Miga MI, Kennedy FE, Weaver JB (1999). An overlapping subzone technique for MR-based elastic property reconstruction. MRM 42:779-786.

65. Van Houten EEW, Miga MI, Weaver JB, Kennedy FE, Paulsen KD (2001). Three-dimensional subzone-based reconstruction algorithm for MR elastography. MRM 45:827-837.

66. Sinkus R, Tanter M, Catheline S, Lorenzen J, Kuhl C, Sondermann E, Fink M (2005). Imaging anisotropic and viscous properties of breast tissue by magnetic resonance-elastography. MRM 53:372-387.

67. Samani A, Plewes DB (2004). A method to measure the hyperelastic parameters of ex vivo breast tissue samples. Phys. Med. Biol. 49 4395-4405.

68. Lawrence AJ, Rossman PJ, Mahowald JL *et al*. (1999). Assessment of breast cancer by MR elastography. Proc ISMRM 7:525.

69. McKnight AL, Kugel JL, Rossman PJ, Manduca A, Hartmann LC, Ehman RL (2002). MR elastography of breast cancer: preliminary results. Amer J Roentgenology 178:1411-1417.

70. Kruse SA, Dresner MA, Rossman PJ *et al*. (1999). 'Palpation of the brain' using MR elastography. Proc ISMRM 7:258.

71. Dresner MA, Rose GH, Rossman PJ *et al*. (2001). Magnetic resonance elastography of skeletal muscle. JMRI 13(2):269-276.

72. Papazoglou S, Braun J, Hamhaber U, Sack I (2005). Two-dimensional waveform analysis in MR elastography of skeletal muscles. Phys Med Bio 50:1313-1325.

73. Rouviere O, Yin M, Dresner MA *et al*. (2005). In vivo MR elastography of the liver: preliminary results. Proc ISMRM 13:340.

74. Peeters F, Sinkus R, Salameh N *et al*. (2005). In vivo MR elastography of liver fibrosis. Proc ISMRM 13:339.

75. Walker CL, Foster FS, Plewes DB (1998). Magnetic resonance imaging of ultrasonic fields. Ultrasound Med Bio 24:137-142.

76. Wu T, Felmlee JP, Greenleaf JF, Riederer SJ, Ehman RL (2001). Assessment of thermal tissue ablations with MRE. MRM 45:80-87.